Thermal Performance Evaluation of a High-Speed Flywheel Energy Storage System

Co Huynh[1], *member IEEE*, Liping Zheng[1*], *member IEEE*, and Patrick McMullen[2]

[1]Calnetix, Inc., Cerritos, CA 90703 USA
[2]Vycon, Yorba Linda, CA 92887 USA
[*]E-mail: lzheng@calnetix.com

Abstract-**This paper presents the loss analysis and thermal performance evaluation of a permanent magnet synchronous motor (PMSM) based high-speed flywheel energy storage system (FESS). The flywheel system is hermetically sealed and operates in a vacuum environment to minimize windage loss created by the large-diameter high-speed flywheel rotor. The rotor is supported by non-contact magnetic bearing system and its loss is dissipated only via radiation to the housing and stationary components surrounding the rotor. 2-D electromagnetic time-step finite element analysis (FEA) with motion was used for rotor loss analysis and lumped-parameter thermal model was used for transient thermal analysis. The rotor loss is simulated based on actual measured motor/generator current waveforms. The simulated temperature distribution meets the measurement quite well. The developed method was also used for sensitivity studies of some crucial system performance parameters.**

I. INTRODUCTION

Thermal analysis has become an important step in design and analysis of electric machines. Thermal analysis is used to predict the temperature rises of the components in order to provide enough margins for safety operation. Lumped-parameter thermal model is a widely used analysis method [1]-[3]. The machine is divided geometrically into a number of lumped components. Each component has a bulk thermal storage and a heat source, and interconnects to neighboring components through a linear mesh of thermal impedances.

In order to predict the thermal performance accurately, it is important to model the machine structure and predict thermal sources as accurately as possible. Electromagnetic 2-D transient finite element analysis (FEA) with motion, and analytical methods were used in calculating rotor and stator losses. When simulating rotor loss using FEA, since the rotor loss is very sensitive to the motor/generator current harmonics, the actual measured current waveforms were used in the simulation model.

Some parameters of the thermal model, such as the interference resistance and radiation emissivity factor, cannot be determined very accurately. Actual testing at various load conditions were carried out to help confirming assumption used in the thermal model for these parameters.

II. FLYWHEEL SYSTEM

Fig. 1 depicts the developed flywheel energy storage system (FESS) which has been used in the UPS market and the crane industry for energy recovery and load leveling. The FESS can provide 140 kW maximum power at 24,000 rpm. The inertia of the rotor with flywheel is 0.683 kg-m^2, and it can store energy of 4.85 MJ at the maximum operating speed of 36,000 rpm. The height of the flywheel housing is 940mm, and the diameter is 350mm. The design details can be found in [4].The flywheel system utilizes patented homopolar permanent magnet biased active magnetic bearings for rotor radial and axial support. The flywheel is hermetically sealed and operates in a vacuum environment to minimize windage loss created by the high-speed flywheel rotor. The rotor loss is removed only via radiation to the housing and stationary components surrounding the rotor.
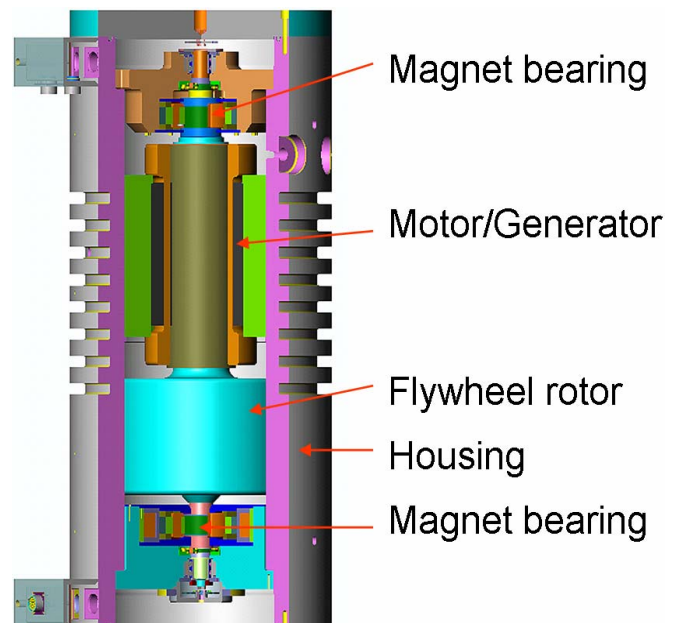
Fig. 1. Cutaway view of the flywheel energy storage system.

The steel hub was chosen over composite technologies to allow for higher rotor operating temperatures, more predictable dynamic performance, and low manufacturing cost. While

composites offer higher energy densities allowing smaller hub designs, lower cost and more predictable dynamic performance with steel hub are considered more important for the target industrial applications. The flywheel housing aligns and supports the bearings and the motor/generator. A vacuum hose valve provides a connection to a vacuum pump required to lower the vacuum level in the flywheel to approximately 4×10^{-3} Torr during operation.

The motor/generator design provides many system benefits including: (a) extremely low rotor losses, (b) low magnetic spring rate with minimal bearing loading due to eccentricity, and (c) robust rotor construction suitable for highly integrated or standalone applications. These benefits, demonstrated for flywheels, extend to other high speed applications such as turbo compressors and turbo alternators.

The two-pole permanent magnet rotor is highly integrated with the flywheel hub, as shown in Fig. 2. The magnet retaining sleeve, made of high strength nonmagnetic alloy, also functions as the main stiffness member for the entire flywheel rotor assembly.

High Speed, High Efficiency Motor/Generator

Energy Storage
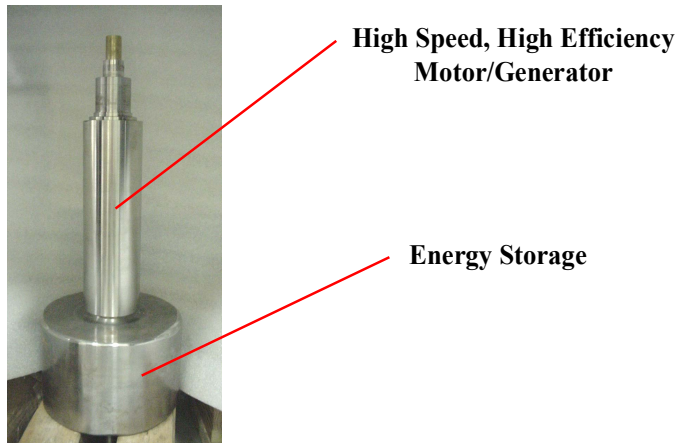
Fig. 2. Permanent magnet rotor integrated with the hub.

III. LOSS ANALYSIS

A. Stator Loss

The stator loss consists of copper winding loss and iron loss. The copper loss includes I^2R loss and eddy current loss. The I^2R loss is calculated at the temperature of 175 °C and the thermal model iterates the heat source of each copper node based on simulated node temperature since the copper loss is temperature dependent. The eddy current loss can be simulated based on FEA or calculated using analytical methods [5], [6].

The iron loss is separated into teeth loss and core loss for more accurate simulation since they are not equally distributed. 2-D time-step transient FEA with motion was used to simulate stator iron loss. The equation used to simulate the iron loss for electric steel is [7]

$$P_C = k_h B_p^2 f + K_c (B_p f)^2 + K_e (B_p f)^{3/2} \qquad (1)$$

where f is the frequency, K_h, K_c and K_e are the coefficients of hysteresis loss, classical eddy current loss, and excess eddy current loss, respectively. The coefficients can be calculated using curve fitting of the iron loss data from manufacturers, by methods of least squares or others, such as genetic algorithm.

B. Rotor Loss

The rotor loss generated by induced eddy current in the steel shaft and permanent magnets is not significant compared to the total loss. However, the rotor loss can only be removed via radiation. Therefore, accurate prediction of rotor loss becomes very important. The major causes of the rotor eddy current loss can be categorized into the following three groups [8]: (a) no-load rotor eddy current loss caused by the existence of slots, (b) on-load rotor eddy current loss induced by the harmonics of windings' magnetomotive force (MMF), which is also called space harmonics, and (c) on-load rotor eddy current loss induced by the time harmonics of the phase currents due to pulse width modulation (PWM). Some analytical methods can also be used to calculate rotor losses [9]-[13]. Reducing slot opening and increasing magnetic gap between rotor and stator can reduce no-load rotor loss. Increasing number of slots per pole and using fractional winding can reduce rotor loss caused by the space harmonics of the winding. Increasing switching frequency and using external line inductors can reduce rotor loss caused by time harmonics of the phase current.

If the eddy current distribution in the rotor is known, the instant rotor power loss can be expressed as

$$P = \int_V \sigma \mathbf{E}^2 \, dV = \int_V \mathbf{J}^2 / \sigma \, dV \qquad (2)$$

where σ is the material conductivity, $\mathbf{E}$ is the electric field, $\mathbf{J}$ is the eddy current density, and V is the volume of the material. The rotor loss is simulated using 2-D FEA transient solver with motion, in which the actual measured motor/generator current waveforms are applied.

IV. THERMAL MODEL

The lumped parameter thermal model is sufficiently detailed to include all the major components and heat transfer mechanisms within the machine without being over complex. Any heat generation due to the losses in the component is regarded as a point source at the node. The thermal model can give the user a clear understanding of the important thermal aspects of the design and which criteria of the design is most sensitive, i.e. rotor losses, rotor radiation emissivity, etc. With this information, the designer can make informed decisions when looking at optimizing the design, especially when compromises must be made.

A volume element is represented by a node in the thermal model, which has mass, thermal capacitance, heat source and thermal resistance to other nearby nodes. The basic laws of conduction, convection, and radiation heat transfer along with the laws of heat storage and the conservation of energy are used. The thermal system is transformed into an electrical analogue nodal network consisting of resistance elements and

sources with specified initial and boundary conditions. Fig. 3 shows one basic node element in the thermal network, where *R1* to *R4* is the thermal resistance to the nearby elements, and *I* is the heat source, and *C* is the thermal capacitance.
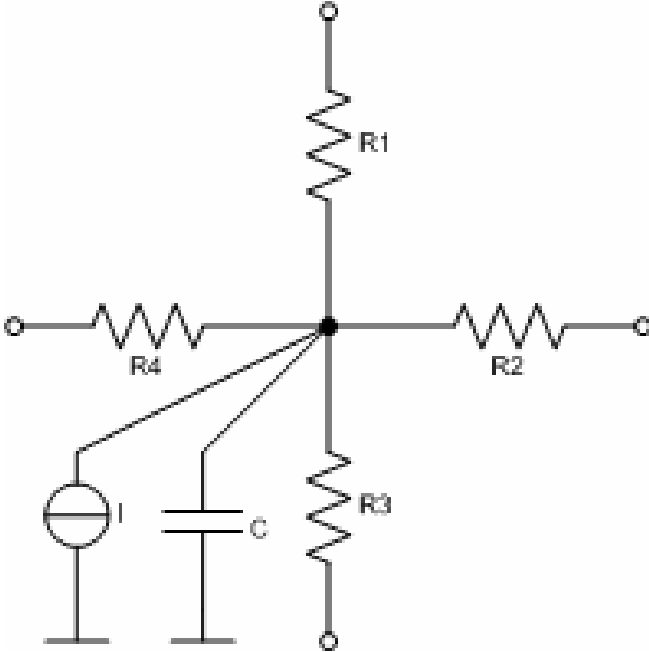
Fig. 3. One node element in the thermal network.

A. Conduction

In a solid body, the heat is transferred from a high temperature region to a low temperature region and is proportional to the temperature gradient. The conduction heat transfer rate, q_{cond}, is expressed as

$$q_{cond} = -kA\frac{\partial T}{\partial x} \tag{3}$$

where k is the thermal conductivity of the material, A is the contact area, and $\partial T/\partial x$ is the temperature gradient in the heat flow direction. The thermal conductivity is about 0.2 W/m/°C for insulation material and as high as 400 W/m/°C for copper winding. For radial gap machine, the heat flow in the axial direction of the stack lamination (lamination direction) can be ignored. The stacking factor has to be considered when calculating effective thermal conduction in radial direction. The model of the copper winding consists of two parts: the copper inside the stack and end-turn winding. For radial machine, the thermal conduction of slot insulation in axial direction is ignored. In radial direction, fill factor is used to calculate the composite thermal condutivity. When modeling the end-turn winding, the surface insulation is considered as separate nodes.

Although there is interference fit between the housing and stator core, there is still some contact resistance due to rough surfaces of stator lamination and housing. The typical interfacial conductance for normal surface finish and moderate contact pressure is 2,200 - 12,000 W/m²/K for aluminum to aluminum interface, and 4,000 - 40,000 W/m²/K for iron to alumi-

num interface [14], [15]. Some analytical methods can also be used to calculate interfacial conductance [16], [17].

B. Convection

Convective heat transfer takes place between a solid source and a fluid. The fluid motion transfers the energy. Convection heat transfer can be expressed using Newton's Law

$$q_{conv} = hA(T_w - T_\infty) \tag{4}$$

where T_w and T_∞ are the solid and fluid temperatures, respectively. For natural convection, the Nusselt number is expressed as

$$Nu = C(GrPr)^n \tag{5}$$

And for forced convection, it is

$$Nu = CRe^m Pr^n \tag{6}$$

where C, m, and n are constants and several useful dimensionless numbers are defined as

Reynolds number $\qquad Re = \rho v L / \mu \qquad (7)$

Grashof number $\qquad Gr = g\beta\Delta T \rho^2 L^3 / \mu^2 \qquad (8)$

Prandtl number $\qquad Pr = Cp\mu / k \qquad (9)$

Nusselt number $\qquad Nu = QL /(kA\Delta T) \qquad (10)$

where Q is the total heat flux, A is the area, μ is the fluid dynamic viscosity, ρ is the fluid density, k is the fluid thermal conductivity, c_p is the fluid specific heat capacity, v is the fluid velocity, ΔT is the delta temperature of the surface, L is the characteristic length of the surface, β is the volumetric coefficient of expansion, and g is the gravitational force of attraction.

C. Radiation

Radiation is the heat transfer mode from a surface due to energy transfer by electromagnetic waves. The net radiant transfer is a function of the optical properties which are strongly dependent on the surface conditions of a given material. Radiative exchange between two surfaces having temperatures T_1, and T_2 and area A_1 and A_2, respectively, can be expressed as [18]:

$$q_{rad} = F_\varepsilon \sigma A_1 (T_1^4 - T_2^4) \tag{11}$$

where σ =5.67e-8 Wm⁻²/k⁻⁴ is the Stefan-Boltzmann constant and F_ε is the gray body view factor, which depends on the geometries of the bodies and the emissivity factors of two surfaces. Materials with different surfaces present different emissivity factors. A black painted rotor has higher emissivity factor than that of the original shinny one.

V. ANALYSIS AND RESULTS

A. Loss Analysis

Harmonics content in the current waveform increases rotor loss, so line inductors are generally used to reduce harmonics. However, the inductance value cannot be too large due to limited terminal voltage, and large inductance will also reduce power factor and increase the weight of the system. To reduce

harmonics at both low current and high current, an 85 uH inductor is connected to each phase. The large inductance value greatly reduces the current harmonics during charging/discharging and dwelling. Fig. 4 plots the measured current waveform when the flywheel is discharging at 16.2 krpm with 50 kW output power, and the corresponding FFT analysis is shown in Fig. 5.
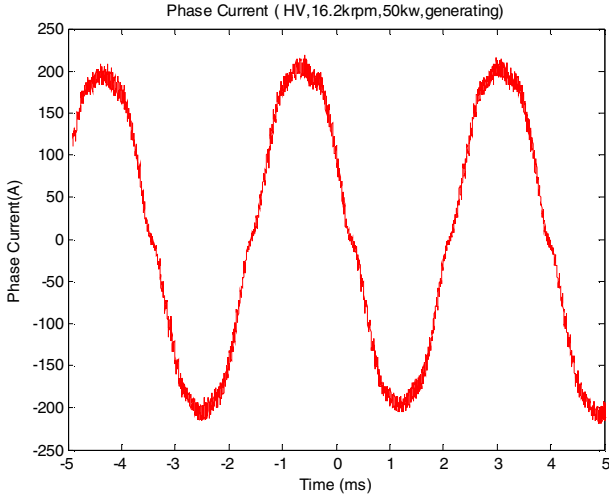
Fig. 4. Measured current waveform at 50 kW discharging.
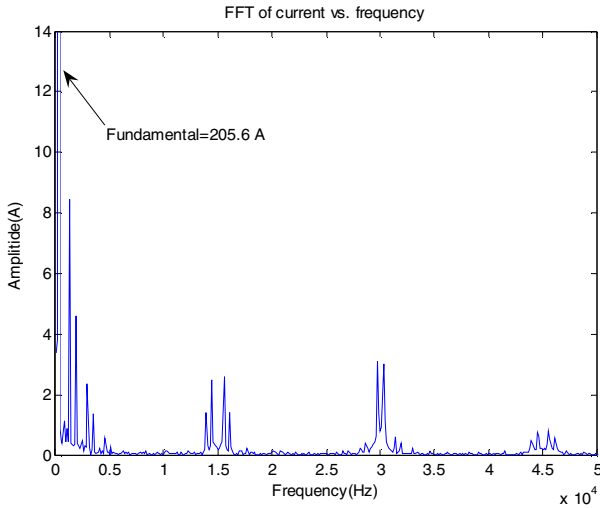
Fig. 5. The corresponding harmonics of Fig. 4.

To accurately predict the rotor loss, the actual measured current waveforms were used in 2-D FEA transient simulation. Fig. 6 plots the simulated eddy current, which is due to stator slot effect, space harmonics and time harmonics of the phase currents, in the metal sleeve and permanent magnet when FESS is discharging at 50 kW at the speed of 16.2 krpm. Fig. 7 shows the simulated loss at different time during 65 seconds cycling (the flywheel spins up from 12 krpm to 18 krpm in 15 seconds, dwells at 18 krpm for 20 seconds, then spins down from 18 krpm to 12 krpm in 20 seconds).

The simulated results were compared to those without low

pass filter, and it is found that low pass filter can reduce rotor loss greatly.
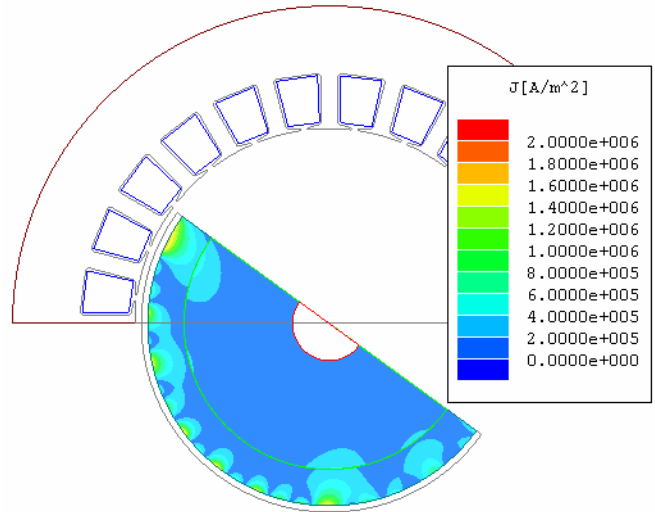
Fig. 6. Simulated eddy current in the metal sleeve and permanent magnet.
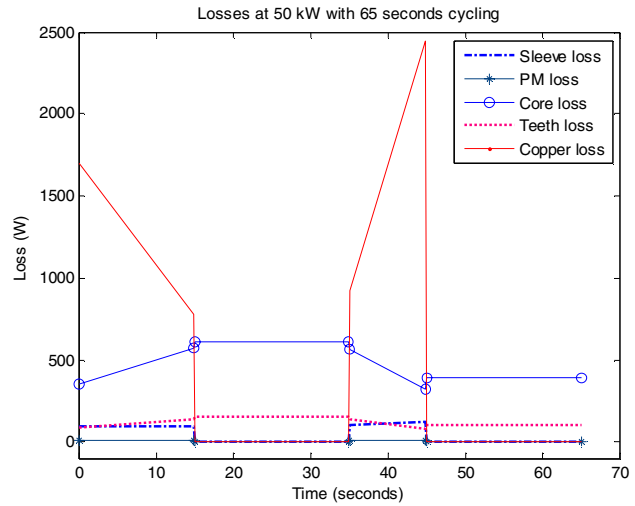
Fig. 7. Calculated flywheel losses vs. time when the flywheel is operating at 65-second cycling with 50 kW output power.

B. Thermal Analysis

The developed thermal model consists of 133 elements. The thermal model parameters, such as rotor emissivity and contact resistance between the housing and stator, were evaluated by running at different load and duty cycle conditions. The thermocouples used to monitor the temperatures at different locations for comparison are shown in Fig. 8, where the rotor permanent magnet temperature is determined based on back EMF changes according to the temperature coefficient of permanent magnet. The measured temperatures for the 50 kW, 65-second cycling case are plotted in Fig. 9. Fig. 10 shows the simulated and measured transient temperatures of the permanent magnet and end-turn winding vs. time when the flywheel is at 65-second cycling with 50 kW output power. Red dot lines repre-

sent the simulation results using the described thermal model, while the blue solid lines are the measurement results. The agreement between them is quite well in this case.
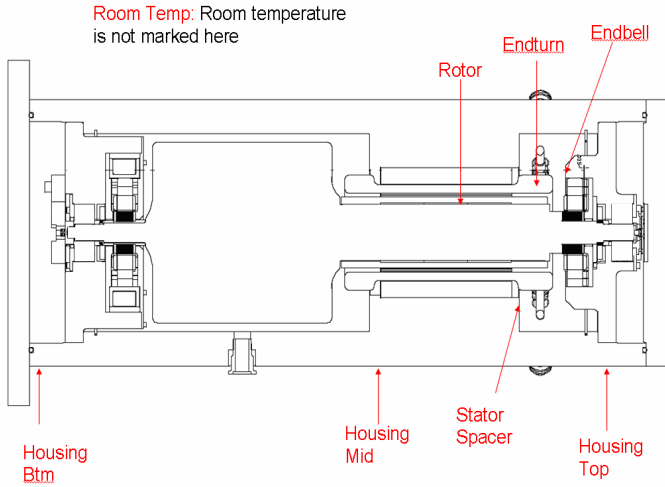
Fig. 8. Locations of the monitored temperatures (the rotor permanent magnet temperature is determined based on back EMF changes, and not sensored by thermocouples).
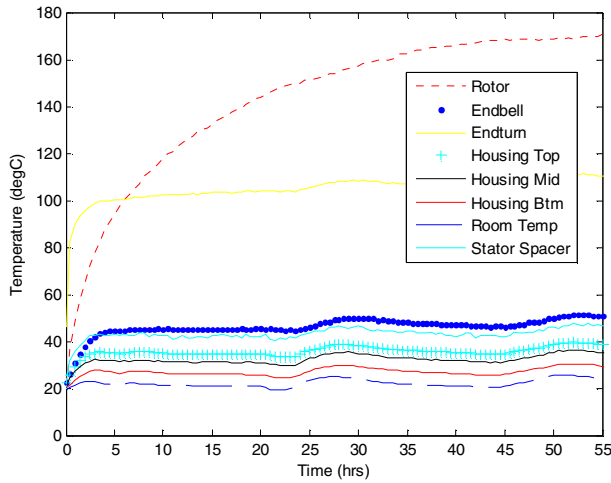
Fig. 9. Measured temperatures when the flywheel is at 65-second cycling with 50 kW output power (with 85 uH & saturated inductors, without emissive coating).

Fig. 11 shows the temperature distribution at steady state. It is found that the rotor temperature is higher at the flywheel top due to smaller radiation surface area. This unit has a shiny rotor. The test result was consistent with a rotor emissivity of about 0.2. The simulation for a flywheel system with emissivity coated flywheel hub and housing was also performed and Fig. 12 shows that the rotor temperature reduces greatly due to large radiation emissivity of the rotor. The test results with coated flywheel housing, hub and rotor was consistent with an emissivity of about 0.9.
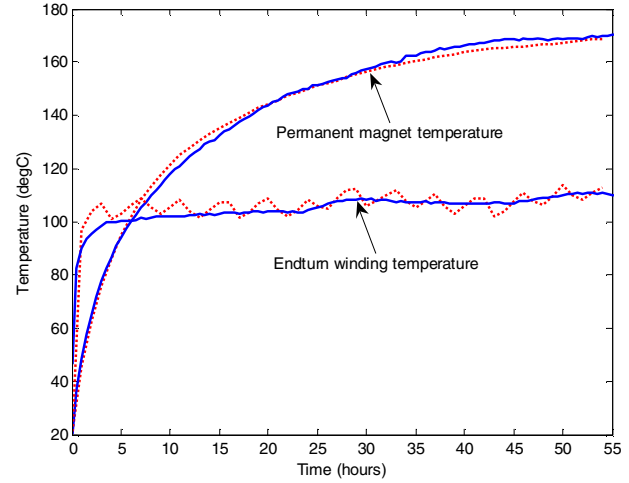
Fig. 10. Simulated and measured temperatures of permanent magnets and stator when 65-second cycling at 50 kW (red dot lines are simulation results and blue solid lines are measured results).
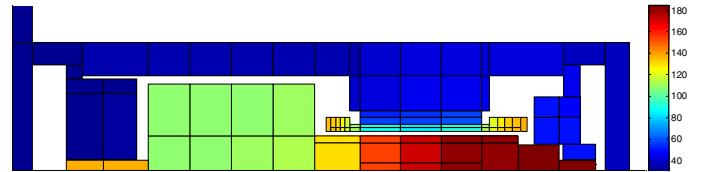
Fig. 11. Steady state temperature distribution of the flywheel system (without emissivity coating) at 50 kW and 65 seconds cycling. The temperature unit is in deg C.
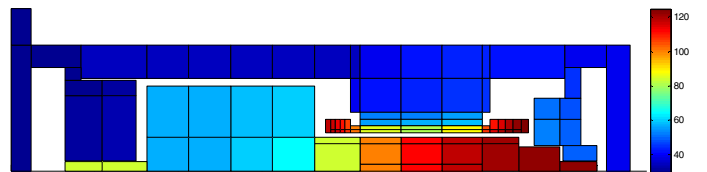
Fig. 12. Steady state temperature distribution of the flywheel system at 50 kW and 65 seconds cycling when the flywheel rotor, stator inner surface, and housing inner surface are coated with high emissivity material. The temperature unit is in deg C.

C. Sensivity Study

The rotor permanent magnet temperature is very critical when targeting for higher power output. It is important to investigate the changes of rotor temperature with the rotor emissivity factor. Fig. 10 shows the permanent magnet temperature at steady state vs. the rotor emissivity factor, from which it is found that improving the rotor emissivity factor can greatly reduce rotor temperature.

From (11), we can also see that when the temperature difference between rotor and stator is close, increasing the emissivity factor is not so effective in further reducing rotor temperature. Although there are still large temperature difference between the flywheel hub and housing, the effective of the thermal conduction is limited by the thermal conduction between motor rotor and flywheel hub.
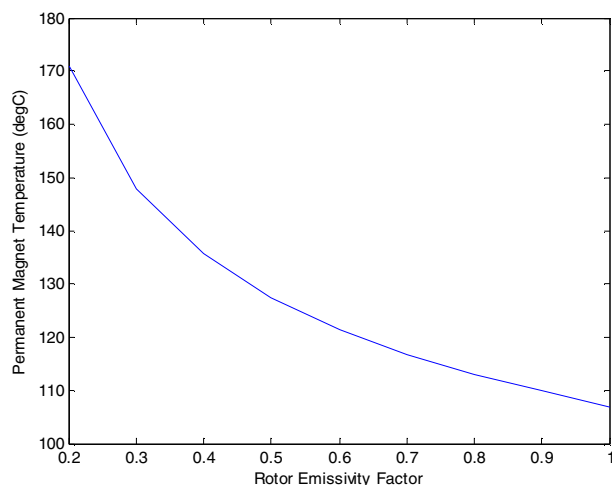
Fig. 13. Simulated steady state permanent magnet temperature vs. rotor emissivity factor.

VI. CONCLUSION

The loss analysis and transient thermal analysis of a permanent magnet synchronous motor based high-speed flywheel energy storage system is presented in this paper. The actual measured current waveforms were used in the rotor loss FEA simulations for more accurate results. The simulation results were compared to the measurements and good agreement was found. The thermal model was also used in doing sensitivity studies with different rotor emissivity factor. The concept of this thermal model can also be used for further high-speed, high-power flywheel energy storage system design considerations

VII. REFERENCES

[1] P.H. Mellor, D. Roberts, and D. R. Turner, "Lumped parameter thermal model for electrical machines of TEFC design," *IEE Proceeding-B,* vol.138, no. 5, Sept. 1991.

[2] M.J., Duran, and J. Fernandez, "Lumped-parameter thermal model for induction machines," *IEEE Trans. Energy Conversion*, vol. 19, no. 4, pp. 791-792, Dec. 2004.

[3] D. Gerling, and G. Dajaku, "Novel lumped-parameter thermal model for electrical systems," *2005 European Conference on Power Electronics and Applications*, 10 pages, 11-14 Sept. 2005

[4] P. T. McMullen, L. A. Hawkins, C. S. Huynh, and D. R. Dang, "Design and development of a 100 kW energy storage flywheel for UPS and power conditioning applications,", *24th International PCIM Conference*, Nuremberg, Germany, May, 2003.

[5] J. Lammeraner and M. Stafl, *Eddy Currents*, CRC Press, Cleveland, Ohio, pp.103-147, 1966.

[6] Spooner, E., and Chalmers, B. J.: ``TORUS': a slotless, toroidal-stator, permanent-magnet generator', *IEE Proc. B Electric Power Appl.*, vol. 139, no. 6, pp.497-506, 1992.

[7] D. Binesti and J. P. Ducreux, "Core losses and efficiency of electrical motors using new magnetic materials," *IEEE Trans. on Magnetics*, vol. 32, no.5, pp. 4887 - 4889, Sept. 1996.

[8] F. Sahin, A. M. Tuckey, and A. J. A. Vandenput, "Design, development and testing of a high-speed axial-flux permanent-magnet machine," *IEEE Ind. Appl. Conf.,* vol. 3, pp.1640-1647, 2001.

[9] Z.Q. Zhu, K .Ng, N. Schofield and D. Howe, "Improved analytical modeling of rotor eddy current loss in brushless machines equipped with surface-mounted permanent magnets," *IEE Proc. Power Appl.* vol. 151, no.6, pp. 641-650, Nov. 2004.

[10] S. M. Abu Sharkh, M. R. Harris, N. Taghizadeh Irenji, "Calculation of rotor eddy-current loss in high-speed PM alternators," *Eighth International Conference on Electrical Machines and Drives*, pp. 170-174, Sept. 1997.

[11] J.L. Kirtley Jr., and E.C. Lovelace, "Drag Loss in Retaining Rings of Permanent Magnet Motors", IEEE International Electric Machines and Drives Conference, 17-20 June 2003.

[12] K. Atallah, D. Howe, P. H. Mellor, and D. A. Stone, "Rotor loss in permanent-magnet brushless AC machines," IEEE Trans. Ind. Applic., vol. 36, no. 6, pp. 1612-1618, Nov/Dec. 2000.

[13] H. Polinder, M.J. Hoeijmakers, "Effect of a shielding cylinder on the rotor losses in a rectifier-loaded PM Machine," *the 2000 IEEE Industry Applications Conference,* vol. 1, pp. 163-170, Rome, 5-10 Oct. 2000.

[14] J. H. Lienhard IV and J. H. Lienhard V, *A Heat Transfer Textbook,* 3rd edition, Phlogiston Press, Cambridge, MA, 2006.

[15] D. Staton, A. Boglietti, and A. Cavagnino, "Solving the More Difficult Aspects of Electric Motor Thermal Analysis in Small and Medium Size Industrial Induction Motors," *IEEE Trans. Energy Conversion*, vol. 20, no. 3, pp. 620-628, Sept. 2005.

[16] M.M. Yovanovich, J.R. Culham, and P. Teertstra, "Calculating Interface Resistance," *Electronics Cooling*, vol. 3, no. 2, pp. 24-29, 1997.

[17] M. Bahrami, J. R. Culham, M. M. Yovanovich, and G. E. Schneider, "Thermal Contact Resistance of Nonconforming Rough Surfaces, Part 1: Contact Mechanics Model," *Journal of Thermophysics and Heat Transfer,* vol. 18, no. 2, April–June 2004.

[18] F. P. Incropera, and D. P. DeWitt, *Fundamental of Heat and Mass Transfer,* 5th ed., John Wiley & Sons, Inc., 2002.